MARS-GCR Analysis for a New Design of Reactor Cavity Cooling System

Yun Je Cho[1)], Hyoung Kyu Cho[2)], Goon Cherl Park[1)]

1) Department of Nuclear Engineering, Seoul National University, San 56-1, Shillim-dong, Kwanak-gu, Seoul, 151-742, Korea
2) Korea Atomic Energy Research Institute (KAERI), 150 Dukjin-dong, Yuseong-gu, Daejeon, 305-353, Korea

ABSTRACT

An investigation of the thermal hydraulic characteristics in a new concept of a reactor cavity cooling system has been carried out using the MARS-GCR code. The proposed RCCS, named a water pool type RCCS, is consists of both passive water pools and active air cooling system to ensure afterheat removal capability as well as to simplify the cavity structures. The calculation was performed for the validation of the capability of MARS-GCR code to simulate multi-dimensional behavior, natural convective heat transfer and radiative heat transfer during normal operation and accident conditions. Based on this assessment, it is concluded that the MARS-GCR code properly predicts the radiative heat transfer in the cavity and the forced convective heat transfer in active air cooling pipes. However, the results show the limitation of the application of the system code with coarse mesh size for the simulation of local phenomenon.

INTRODUCTION

The reactor cavity cooling system (RCCS) is a passive decay heat removal system for high temperature gas-cooled reactors (HTGRs) installed in the cavity between the reactor vessel and concrete wall of the containment. The objectives of RCCS are to remove the parasitic heat losses during normal operation and all of the core afterheat in the unlikely case of failure or unavailability of all other shutdown cooling systems [1].

A new concept of RCCS for HTGRs called the water pool type RCCS was proposed at Seoul National University (SNU) in order to overcome the disadvantages of the existing RCCS types. This system is expected to have better cooling capability than the air cooled type RCCS and to benefit from a simpler cavity configuration than the existing water cooled type RCCS [2, 3].

A simple system with a passive water pool was utilized to strike a balance between the weak cooling ability of the air cooled RCCS and the complex structures of the water cooled RCCS. Utilizing the water pool has the advantage that the good heat removal capability of water can be utilized without any complex geometrical structures. In this system, the heat removal takes place first inside the reactor core. Next, the heat is transferred from the uninsulated reactor vessel to the water pools primarily by radiation from the hot vessel surface to the relatively cold cavity surfaces, and partly by the natural convection of air in the enclosed cavity [4]. Finally, the heat is transported and rejected to the atmosphere by the air forced convection of air cooling pipe during the normal operation condition and latent heat of the water in the water pools during the accident condition. By using the atmosphere as an ultimate heat sink, it is possible to eliminate the need for an additional cooling loop under normal operation conditions.

In the case of an accident involving the loss of forced convection caused by the unavailability of the main reactor core cooling system, including the forced air cooling system of the RCCS, the proposed system uses water pools as a heat sink to remove the afterheat. In this case, the afterheat is passively absorbed by heating up and boiling off the water in the water pools, and the steam generated in the water pools is released to the atmosphere.

As a previous work, three categories of experiments were performed to find the information to be used for the assessment of the MARS-GCR code for the proposed water pool type RCCS. The experiments fall into three categories: the emissivity measurement test [5], separate effect test (SET) for a quarter of water pool of the RCCS-SNU facility [6], and integral effect test (IET) with the RCCS-SNU facility. In our previous studies, we determined the emissivity of the reactor vessel wall in the emissivity measurement test. In addition, the proper correlations for the pressure drop along the cooling pipe and convective heat transfer by air forced flow in the cooling pipe were found with the MARS-GCR code assessment via the SET for a quarter water pool of the RCCS-SNU facility. Then, the experimental data from the IET for the RCCS-SNU facility were utilized to validate the capability of the MARS-GCR code to simulate the various heat transfer modes, namely forced convection, natural convection and radiative heat transfer.

The MARS code, which has been developed at Korea Atomic Energy Research Institute by consolidating and restructuring the RELAP5/MOD3.2 [7] and COBRA-TF [8], has the capability of analyzing the one-dimensional or three-dimensional best estimated thermal hydraulic system and the fuel responses of the light water reactor transients. The one-dimensional module of the MARS code is based on the RELAP5 code. As such the basic field equations, constitutive relations, and thermal hydraulic models of the one-dimensional module of the MARS are essentially the same as those of the RELAP5. And multi-dimensional modeling and analysis capabilities have been added to the RELAP5, thus enabling MARS to be used for applications where a multi-dimensional analysis is needed. The enhanced version of MARS, MARS-GCR, is a viable tool for the thermal-hydraulic analysis of a gas-cooled reactor, since it is not only capable of calculating the gas properties accurately, but is also robust and flexible enough to simulate the various

transients [9, 10].

Through the assessment of MARS-GCR code, we validated the capability of MARS-GCR code to simulate the pressure drop and forced convective heat transfer in the cooling pipes. In addition, the multi-dimensional flow, natural convective heat transfer, thermal stratification inside the cavity and water pool, and radiative heat transfer in the cavity were also examined.

DESCRIPTION FOR THE RCCS-SNU FACILITY

Figure 1 shows a schematic diagram of the RCCS-SNU test facility. The reactor vessel used in the test facility is a simplified model of the PBMR reactor vessel and the cross vessel which connects the reactor vessel and recuperator was not simulated. The total height of the test facility is 2.6 m and its outer diameter is 0.75 m. In the reactor vessel, six heater rods are installed to simulate the heat loss and the afterheat. As shown in Fig. 1, the RCCS-SNU facility consists of the reactor vessel with 6 heater rods, a cavity, a side water pool surrounding the vessel, an upper water pool, 13 cooling pipes with 11 U-bends submerged in the side water pool and upper water pool. One air cooling pipe is installed in the upper water pool and 12 pipes are submerged in the side water pool. The outlets of the pipes are connected to an air blower system. Ambient air inhaled at the inlet of the cooling pipes absorbs the heat from the side and upper water pools and releases the heat into the atmosphere. The water pools receive the heat from the reactor vessel wall via convection and radiative heat transfer.

The experiments consisted of nine test cases for normal operation condition with varying the heater power and air inlet velocity as shown in Table 1. The experiments for normal operation conditions were carried out with heat losses of 0.35 % (9.3 kW), 0.94 % (25 kW) and 1.51 % (40kW) of normal power and air velocities of 20 m/s, 30 m/s and 40 m/s.

Once heat balance was achieved in the normal operation condition, the Loss of Forced Convection (LOFC) tests were started. The initial steady state temperature of the water pool was 63 ℃ with a heat loss fraction of 0.35%. All of the forced air cooling systems were stopped at the beginning of the LOFC test and the afterheat was passively removed by sensible heat transfer or latent heat transfer in the water pools. The previous analysis result for 450MW MHTGR [6] was used to determine the experimental conditions of the afterheat transient. Figure 2 shows the transient of the afterheat removal rate for the RCCS in the MHTGR and the transient of the heater power in the experiments designed to simulate the afterheat. The actual heater power in the LOFC experiments was obtained by adding the heat loss (0.35 %) to the afterheat transient. In order to accentuate the depletion of the side pool and upper pool in the boiling situation, the safety valves installed in the water pools were manually opened when the water in the water pools reached the saturation temperature.

As a result, detailed information on the temperature distribution and heat removal fraction of the water pools were obtained. In addition, we found that the maximum temperature of the reactor vessel was kept below the design limitation suggested for the PBMR.

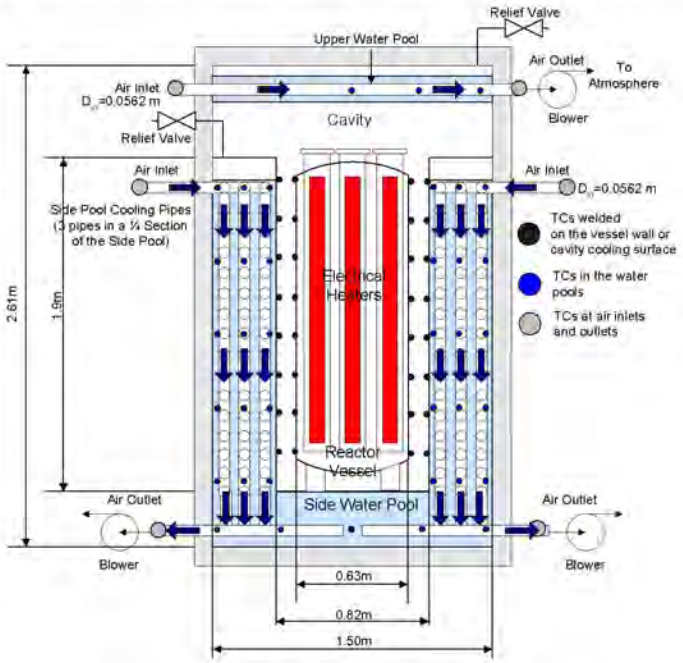

Fig. 1. Schematic Diagram of the RCCS-SNU Facility

Table 1. Test Matrix for IET

	HEATER POWER		AIR VELOCITY	
Normal Operation	Q10	9.3 kW (0.35 %)	V20	20 m/s
			V30	30 m/s
			V40	40 m/s
	Q25	25 kW (0.94 %)	V20	20 m/s
			V30	30 m/s
			V40	40 m/s
	Q40	40 kW (1.51 %)	V20	20 m/s
			V30	30 m/s
			V40	40 m/s
LOFC Accident	LOFC	10 kW (0.35 %) + Afterheat	N/A	0 m/s

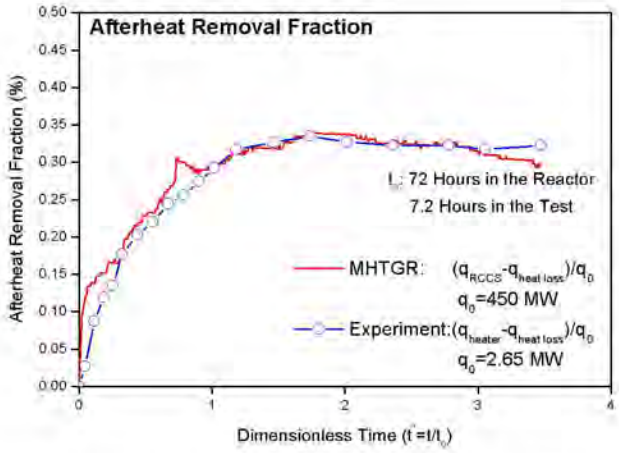

Fig. 2. Transient of Afterheat Removal Rate by RCCS

ANALYSIS MODEL AND BOUNDARY CONDITIONS

Nodalization

Figure 3 shows the MARS-GCR model used to simulate the RCCS-SNU test facility. The detailed structures inside the reactor vessel are not simulated in the model. Instead, the boundary condition of constant heat flux is applied to the reactor vessel wall. The side water pool (MD100) is nodalized with a multi-dimensional component consisting of 8 x 4 x 6 (r-θ-z) nodes in cylindrical coordinates. In particular, small size nodes are generated near the inner wall of the side water pool to simulate the steep temperature gradient near wall. In order to determine the node size near wall, as a preliminary work, the thermal boundary layer was calculated with simple correlation [11], and the result showed that the thermal boundary layer has about the thickness of 5 mm. The bottom water pool (MD120), the upper water pool (MD150) and the cavity are also modeled with multi-dimensional components. The air cooling pipes (from Pipe401 to Pipe 443) are modeled with 13 pipe components (one in the upper water pool and 12 in the side and bottom pools). The air is inhaled at the inlet of each pipe component by connecting the time dependent junction at the outlet of the cooling pipes with a constant mass flux boundary condition.

For the calculation of the radiative heat transfer, the MARS-GCR code needs the emissivities and view factors for all of the radiating heat surfaces that participate in this process [12]. The emissivities were obtained from the results of the emissivity measurement test. The view factors of the surfaces of the radiation enclosure are calculated by the

commercial code, Net Energy Verification and Determination Analyzer (NEVADA), with the Monte-Carlo mathematical technique within a 97 % confidence level [13]. A total of 96 surfaces are considered for the radiation enclosure between the outer surfaces of the reactor vessel and inner surfaces of the water pools, as described in Fig. 4. The bottom and side surfaces of the side water pool and bottom surface of the upper water pool are divided into 12 (1-12), 28 (13-40) and 8 (49-56) surfaces, respectively. The side surfaces of the upper cavity and interfacial surfaces between the upper cavity and side water pool are modeled with 8 (41-48) and 12 (57-72) surfaces, respectively. The upper and bottom surfaces of the reactor vessel are modeled with 4 (73-76, 93–96) surfaces and the side surfaces of the reactor vessel with 16 (77-92) surfaces.

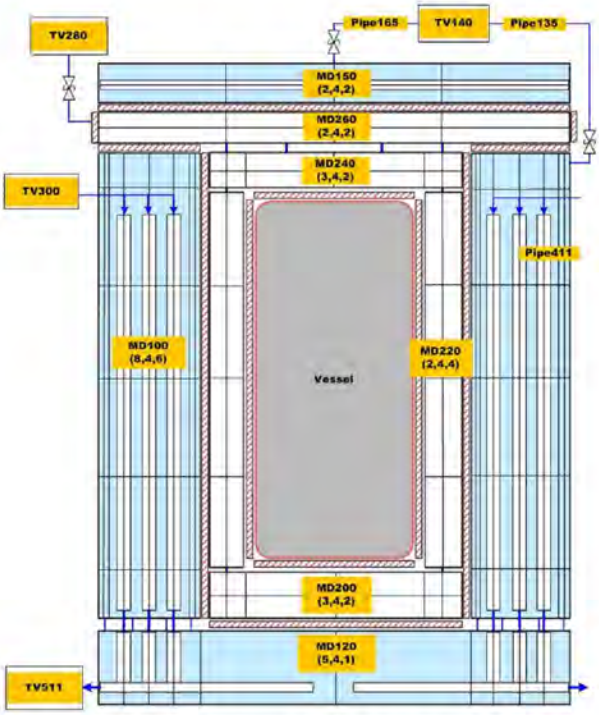

Fig. 3. Nodalization for MARS-GCR Analysis of RCCS-SNU Facility

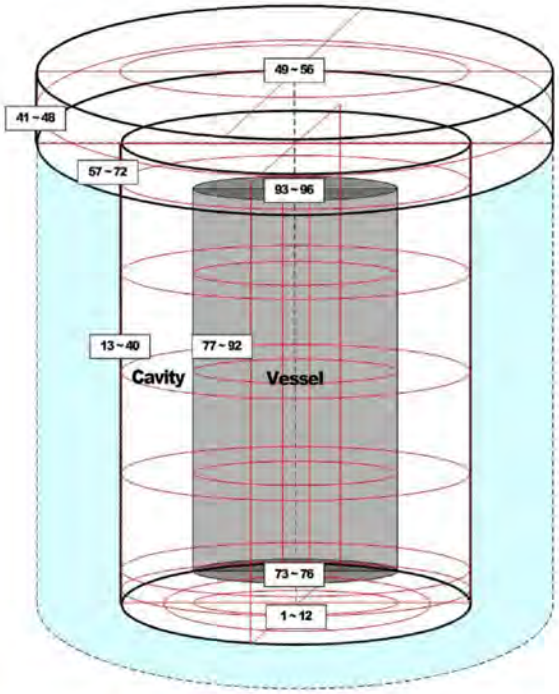

Fig. 4. Schematics of the Radiation Enclosure for Analysis of Radiative Heat Transfer

Boundary Conditions

In the calculation for the normal operation condition, constant heat flux boundary conditions are specified on the reactor vessel wall to simulate the heater power. Constant temperature and mass flux boundary conditions are applied to the air inflow from the inlet of the cooling pipes. In addition, Hooper's correlation [14] and Mori-Nakayama's correlation [15] with the modified helical circle diameter are applied to the air cooling pipes to simulate the pressure drop and the forced convective heat transfer, respectively.

On the other hand, for the LOFC calculation, we want to focus our concern on the thermal hydraulic phenomenon inside water pool, especially subcooled boiling, nucleate boiling near the wall and water level reduction. For the sake of this purpose, the analysis was performed with only side and bottom water pool (MD100, MD120) with temperature boundary condition on the inner wall of side water pool.

$$\bar{h} = Nu_L \frac{k}{L}$$

Where, $$Nu_L = \left\{ 0.825 + \frac{0.387\left(Ra_L\right)^{\frac{1}{6}}}{\left[1+\left(\frac{0.492}{\mathrm{Pr}}\right)^{\frac{9}{16}}\right]^{\frac{8}{27}}} \right\}^2 \quad (1)$$

If the default geometry type is applied to the inner wall of the side water pool as the boundary condition, the MARS-GCR code uses the Chuchill-Chu correlation, shown in Eq. (1), developed for the simulation of natural convective heat transfer on a vertical plate [15, 16]. Because the side water pool of the RCCS-SNU facility is not a single plate, but an annulus enclosure, therefore, the heat transfer coefficient table calculated using the effective thermal conductivity, proposed by Raithby and Hollands for the heat transfer by natural convection in a long horizontal annulus [17], is applied on the inner wall of the side water pool, as shown in Eq. (2).

$$\bar{h} = \frac{k_{eff}}{D_i \ln\left(\frac{D_o}{D_i}\right)}$$

$$\text{Where,} \quad \frac{k_{eff}}{k} = 0.386\left(\frac{\Pr}{0.861+\Pr}\right)^{\frac{1}{4}}\left(Ra_c^*\right)^{\frac{1}{4}}$$

$$Ra_c^* = \frac{\left[\ln\left(\frac{D_o}{D_i}\right)\right]^4}{L^3\left(D_i^{-\frac{3}{5}}+D_o^{-\frac{3}{5}}\right)^5} Ra_L \qquad (2)$$

However, for the LOFC calculation, Eq. (2) cannot be applied for entire calculation time because Eq. (2) was developed for single phase condition. Therefore, the heat transfer coefficient table calculated using the effective thermal conductivity is applied only before the vaporization by subcooled boiling on the wall become significant. Then, after subcooled boiling occurred near the wall, the default geometry type is used in two phase heat transfer region.

RESULTS AND DISCUSSION

Normal Operation Conditions

The analysis results obtained using the two different boundary conditions on the inner wall of the side water pool mentioned above are compared in Figs. 5 to 8 for the case where the heat loss is 0.35 % of the normal power (9.3 kW) and the air velocity at the inlet of the cooling pipe is 20 m/s. The overall calculated results with the two different boundary conditions are similar to each other, except for the temperature distribution of the cavity wall as shown in Fig. 5.

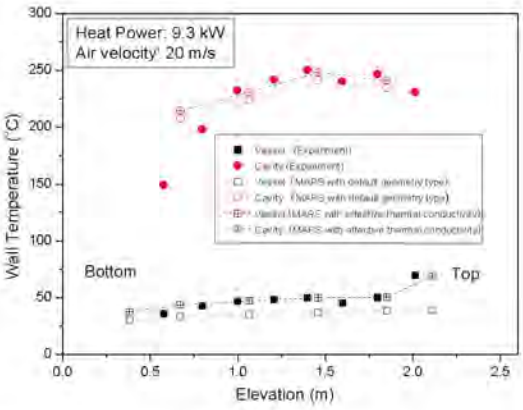

Fig. 5. Temperature Distribution of Cavity and Vessel Wall (Heat loss: 9.3 kW, Air velocity: 20 m/s)

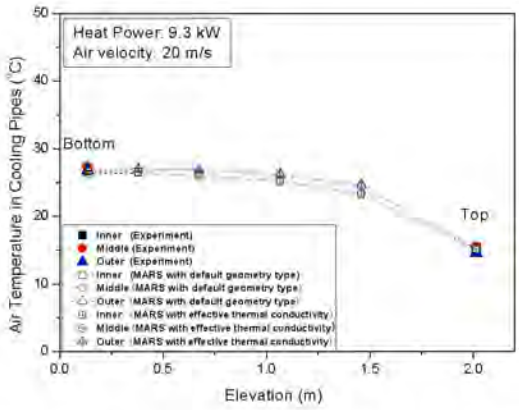

Fig. 6. Temperature Distribution of Air in Cooling Pipes (Heat loss: 9.3 kW, Air velocity: 20 m/s)

The analysis result for the temperature distribution on the inner wall of the side water pool with the default geometry type shows lower temperature ranges than the experimental results, especially at the highest elevation of the side cavity wall, because the MARS-GCR code with the default geometry type overestimates the heat transfer coefficient by natural convection in the enclosure. However, the analysis results are improved when the heat transfer coefficient calculated with the effective thermal conductivity developed for natural convection in the horizontal annulus enclosure is applied.

The temperature distribution of the vessel wall except the bottom region is properly estimated, and the peak temperature and where it occurs are also estimated well. However, the temperature of the vessel wall at the bottom region

is slightly over-predicted because of the discrepancy for simulation of the thermal stratification phenomenon inside the cavity.

Figure 6 gives the temperature distributions of the air in the cooling pipes installed at three radial positions. The air inhaled from the inlet of the cooling pipe receives a large amount of thermal energy in the upper region of the side water pool, with the result that the air temperature is rapidly increased in this region. As the air flows downward, the temperature of the air shows an almost flat tendency. The analysis results agree well with the experimental results measured in the inlet and outlet of the cooling pipes.

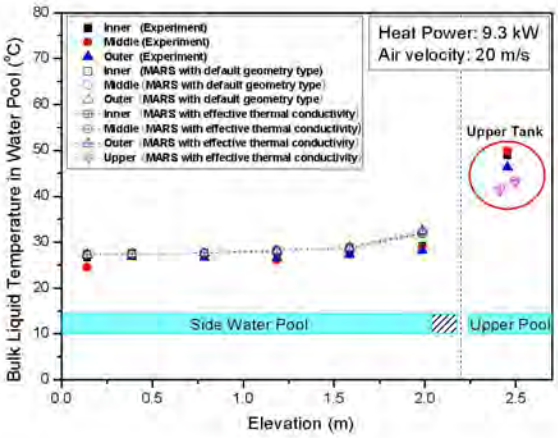

Fig. 7. Temperature Distribution of Water in Water Pool (Heat loss: 9.3 kW, Air velocity: 20 m/s)

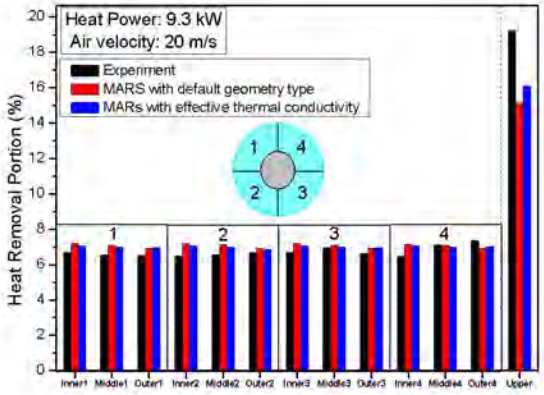

Fig. 8. Comparison for Heat Removal Fraction (Heat loss: 9.3 kW, Air velocity: 20 m/s)

Figure 7 shows the temperature distributions of the bulk liquid measured at three different radial positions, viz. the inner part (10mm from the inner wall of the side water pool), middle part (at the center of the side water pool) and outer part (10 mm from the outer wall), along the elevation in the side and upper water pools. In the side water pool, the highest temperature is observed at the top of the side water pool, where the free surface between steam and water exists in both the calculated and experimental results. However, the calculated result slightly overestimates the bulk liquid temperature at the top of the pool. The other nodes, below the top of the pool, show a temperature variation of less than 2 ℃ with changing elevation. Moreover, the difference of the liquid temperature between the inner part and outer part of the water pool is also less than 2 ℃. These results are explained by the characteristics of the system, in which relatively cold ambient air is inhaled from the top part of the water pool. These characteristics allow temperature distribution of bulk liquid to be almost uniform in the side water pool while the analysis result of the bulk liquid temperature in the upper water pool was slightly lower than the experimental result.

This trend is exemplified by Fig. 8 showing the heat removal fraction in each cooling pipe. The experimental results for the fraction of heat removed by the 12 cooling pipes inside the side water pool show some variation within a maximum deviation of 0.85%. The MARS-GCR analysis result also predicts an almost constant heat removal fraction in the 12 pipes inside the side water pool. On the other hand, the fraction of heat removed by the cooling pipe inside the upper water pool was under-predicted and it is assumed that the discrepancy is due to the incapability of the MARS-GCR code to correctly simulate the heat transfer by natural convection, especially the thermal stratification phenomenon in the enclosure. This presumption is supported by the tendency for the difference in the fraction of heat removed by the upper water pool between the analysis and experimental results to decrease with increasing heater power when the fraction of convection in the total heat transfer is reduced.

The MARS-GCR analysis for all of the test cases listed in Table 1 was performed using the heat transfer coefficient on the inner wall of side water pool calculated with the effective thermal conductivity. The results obtained for the temperature distributions of air in the cooling pipe, pipe wall, liquid bulk, and reactor vessel and cavity wall for all of these cases show a similar tendency to those of the cases depicted in Figs. 5 to 8 except for that of the upper water pool. The temperatures of the bulk liquid in the upper water pool calculated by the MARS-GCR code are underestimated by about 20 %, and this discrepancy is attributed to the incorrect calculation of the heat removal fraction.

LOFC Accident Condition

Figure 9 shows the temperature transient of water in the side water pool at different axial positions. Before the vapor is generated at the top node, the heat transfer coefficient table calculated using the effective thermal conductivity was used for single phase heat transfer. As shown in Fig. 9, the MARS-GCR properly predicts the temperature transient

around before 6000 second. Then, if the vapor generated by subcooled boiling at the top node becomes large enough, the default geometry type is implemented for two phase heat transfer. When the default geometry type is used, MARS-GCR code over-predicts the heat transfer from the cavity wall to the water pool, so that the water temperatures in the side pool show slightly higher values than the experimental data.

As mentioned in the calculation result for normal operation conditions, the discrepancy related to the thermal stratification phenomenon is also found. The water temperature at the top node increases slightly faster than experimental data. Especially, the temperature of water in the lower region of the water tank shows the large discrepancy between calculation and experimental results. It means that the water in the lower region is mixed well compared to experiment, and it makes the temperature of water at the top node reach to the saturation temperature faster than experiment. The cause of this result is assumed that the numerical diffusion due to coarse node size produces qualitatively incorrect results.

Because the calculated temperature at the top node reaches to the saturation temperature faster than experimental result, it also affects the changing rate of water level in the side water pool as shown in Fig. 10. The decreasing rate of water level calculated by MARS-GCR code is slightly larger than experimental data and it is estimated that the vapor generation by subcooled boiling near wall in the water pool, where the buoyancy driven natural convective heat transfer is major heat transfer mechanism, is slightly over-estimated by the code.

The safety valve installed in the side water pools is manually opened when the temperature of water in upper region of the side water pools reaches the saturation temperature. The valve opening time calculated by MARS-GCR code is 25600 second, while the experimental data shows 27000 second.

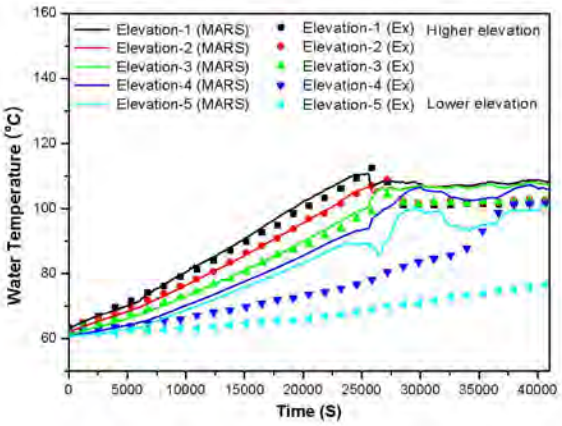

Fig. 9. Temperature Transient of Water in Side Water Pool (LOFC)

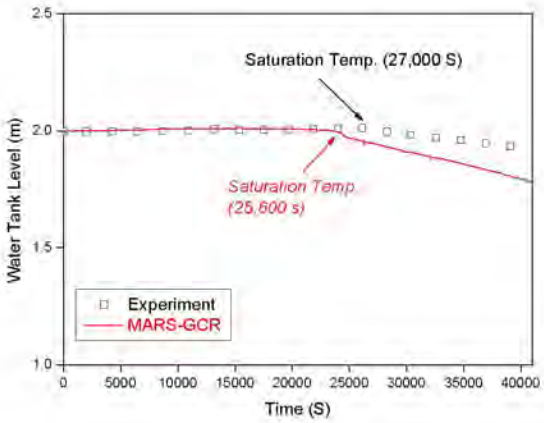

Fig. 10. Transient of Water Level in the Side Water Pool (LOFC)

SUMMARY AND CONCLUSION

In this paper, we validated the capability of MARS-GCR code to simulate the thermal hydraulic behavior in the proposed new type of RCCS. For this purpose, the assessment of the MARS-GCR code was performed as the RCCS-SNU test facility was modeled and simulated using the MARS-GCR code. The Mori-Nakayama correlation and heat transfer coefficient derived from the effective thermal conductivity were applied for the simulation of the forced convective and natural convective heat transfer, respectively. In the calculation, the radiative heat transfer is also included using the emissivity and view factors of the surfaces in the radiative enclosure.

As the results, the temperature distributions of air in the cooling pipes, pipe wall, liquid bulk and reactor vessel and cavity wall were reasonably predicted by the MARS-GCR code. However, the analysis results for the thermal stratification phenomenon inside the cavity and water pool show a discrepancy associated with the use of a coarse node size. In the LOFC calculation, decreasing rate of water level in the side water pool shows faster tendency compared to the experiment, and it is estimated that code over-estimates the vapor generation rate by subcooled boiling near wall in the water pool where the buoyancy driven natural convective heat transfer is major heat transfer mechanism.

Consequently, it is concluded that the development of a new model which can be applied to system codes is necessary in order to reasonably simulate the subcooled boiling near wall as well as the thermal stratification phenomenon in enclosures. The developed model will be utilized to simulate the LOFC accident experiment with the RCCS-SNU facility, but also to optimize the design of the proposed water pool type RCCS, viz. the configuration of air cooling pipe, pumping power of the air blower and the size of the water pools using the MARS-GCR code.

NOMENCLATURE

D_i : Inner Diameter of Annulus
D_o : Outer Diameter of Annulus
H : Height of Cavity
$\bar{h}$: Averaged Heat Transfer Coefficient
k : Thermal Conductivity
k_{eff} : Effective Thermal Conductivity
L : Gap Length of Cavity
Nu_L : Nusselt Number
Pr : Prandtl Number
$R1,R2$: Radius of Curvatures
Ra_L : Rayleigh Number
Ra_c^* : Modified Rayleigh Number

REFERENCE

1. "Heat Transport and Afterheat Removal for Gas Cooled Reactors under Accident Conditions," IAEA-TECDOC-1163, International Atomic Energy Agency, 2000.
2. Zuying Gao, Shuyan He, Min Zhang, "Afterheat Removal for HTR-10 Test Module under Accident Conditions," *Specialists meeting on decay heat removal and heat transfer under normal and accident conditions in gas cooled reactors*, Juelich, Germany, 1992.
3. Cho, H. K. Cho, Y. J. Park, G. C., "Experiments on a Water Pool Type Reactor Cavity Cooling System in a High Temperature Gas Cooled Reactor," *Nuclear Technology*, In Press
4. "Passive Decay and Residual Heat Removal in the MHTGR," IAEA-TECDOC-757, International Atomic Energy Agency, 1982.
5. Cho, Y. J. Kim, M. O. Park, G. C., "Experimental Study on Measurement of Emissivity for Analysis of SNU-RCCS," *Nuclear Engineering and Technology*, Vol. 38, 2006, pp. 99-108.
6. Park, G. C. Cho, Y. J. Cho, H. K., "Assessment of a New Design for a Reactor Cavity Cooling System in a Very High Temperature Gas-Cooled Reactor," *Nuclear Engineering and Technology*, Vol. 38, 2006, pp. 45-60.
7. *RELAP5/MOD3 Code Manual*, NUREG/CR-5535, USNRC, 1988.
8. Thurgood, M.J., et al., "COBRA-TF: a thermal-hydraulics code for transient analysis of Nuclear Reactor Vessel and Primary Coolant Systems," NUREG/CR-3046, USNRC, 1983.
9. Lee, W. J. Bae, S.W. Chung, B.D., "Validation of one-dimensional module of MARS 2.1 computer code by comparing with the RELAP5/MOD3.3 developmental results," KAERI/TR-2411/2003, KAERI, Daejeon, Korea, 2003.
10. Lee, W. J., "Development of MARS-GCR/V1 for Thermal-Hydraulic Safety Analysis of Gas-cooled Reactor System," *Nuclear Engineering and Technology*, Vol. 37, 2005, pp. 587.
11. Kimura, S. Bejan, A., "The Boundary Layer Natural Convection Regime in a Rectangular Cavity with Uniform Heat Flux from the Side," *Transactions of the ASME*, Vol. 106, 1984, pp. 98.
12. Modest, M. F., *Radiative Heat Transfer*, Academic Press, USA, 1993.
13. *NEVADA Software Package Reference Manual*, TAC Technologies, USA, 1999.
14. Hooper, W. D., "The Two-K Method Predicts Head Losses in Pipe Fittings," *Chemical Engineering*, Vol. 24, 1981, pp. 96.
15. "RELAP5/MOD3 Code Manual Volume IV: Models and Correlations," NUREG/CR-5535, Idaho National Engineering Laboratory, 1995.
16. Churchill, S. W., "Free Convection in Layers and Enclosures," *Heat Exchanger Design Handbook*, Section 2.5.8, 1984.
17. Frank P. Incropera, David P. Dewitt, *Introduction to Heat Transfer*, Third Edition, John Wiley & Sons, pp. 474, 1996.